Investigation of self-adaptive algebraic tomography for gas reconstruction in larger temperature range by multiple wavelengths absorption spectroscopy

Ning Li (李 宁)*, Xiaojing Lv (吕晓静), and Chunsheng Weng (翁春生)

National Key Laboratory of Transient Physics, Nanjing University of Science and Technology, Nanjing 210094, China

**Corresponding author: stokim@gmail.com*

Received August 28, 2014; accepted October 24, 2014; posted online November 28, 2014

We develop a self-adaptive algebraic tomography algorithm (SAATA) to investigate the simultaneous reconstruction of concentration and temperature distributions in larger temperature range from two views. The simplified optical arrangement with fewer projections is realized by extension of spectral information at multiple wavelengths, resulting in great potential in applications of practical combustion diagnosis. The results show SAATA can perform much better reconstructions in 300–3000 K temperature range than genetic simulated annealing algorithm and least-square orthogonal-triangular decomposition method with two-wavelength scheme. More phantoms are created to demonstrate the capability of SAATA to capture the peaks and adapt for both flat and sharp temperature distributions. Meanwhile, the advantage of high stability ensures better reconstruction performance at noise levels from 0.1% to 10% in projections.

OCIS codes: 110.2960, 120.1740, 280.3420, 300.6260.

doi: 10.3788/COL201412.121103.

Line-of-sight gas measurement by tunable diode laser absorption spectroscopy has been widely applied to many fields[1–4]. The increasing demand of spatially resolved measurements plays an important role in encouraging the research on distribution properties for nonuniform flows. Unlike CCD tomography reconstruction scheme, the inherent characteristic of tunable diode laser sensing makes it more difficult to achieve spatially resolved measurements. A large number of projections are required for a satisfactory tomographic reconstruction, leading to a complex optical system including a larger number of laser-detector pairs from views around the domain of interest in all directions[5]. These requirements severely limit the application of tomographic technique in practical combustion diagnosis, and significantly restrict the imaging capability and applicable field of the tomographic technique[6]. In spite of enough projection acquisition, the designed optical system by scanning mode of mechanically rotating or swing computed tomography[7] is hardly introduced into the practical application in combustion due to the complexity and inadequate temporal resolution. Fixed optical arrangement with stationary projections is the most promising way to perform reconstructions in the dynamic combustion.

One of the vital issues with regard to the reconstruction imaging capability and computation is optics design. Terzija *et al.* proposed a hitherto unreported design criterion for optimal beam geometry[8]. Daun *et al.* developed a rigorously defined algorithm for optimizing the beam arrangement using the properties of the resolution matrix[9]. Song *et al.* also gave a factor to evaluate the beam arrays relating to the discrete region[10]. The other issue is the effective algorithm to improve reconstruction imaging capability based on the incomplete projections and reduce computation. Past efforts predominantly relied on the use of one or two wavelengths to obtain chemical species distribution[11–13]. Recently, Daun *et al.* developed level set method to solve the limited projection tomography problem[14]. The advances in laser sources and wavelength-division multiplexing (WDM) technique enable a promising outlook to overcome these limitations by extension of spectral information in single projection[15,16]. That would be an effective way to improve the reconstruction of high quality and reduce the number of projections required potentially. However, multiple wavelengths scheme is often introduced into the optimization algorithm with much computation for searching, such as the hyperspectral tomography based on simulated annealing (SA) with 10 wavelengths to reduce the projections and obtain reconstruction over a wide range of noise levels as given in Ref. [17]. Li *et al.* proposed a hybrid optimization algorithm based on genetic SA algorithm (GSAA) to obtain the global optimization results using four wavelengths scheme by 32 rays[18].

In this letter, multiple wavelengths scheme is introduced into the developed self-adaptive algebraic tomography algorithm (SAATA) to obtain a satisfactory reconstruction based on a simplified optics design with less computation. The restricted number of projections is reduced by extension of spectral information from four selected candidate transitions to cover a much larger temperature range. Significant advantages of SAATA are demonstrated in the following aspects: 1) simultaneous concentration and temperature reconstructions with incomplete projections from only two views; 2) self-adaptive adjustment behavior to

maintain high sensitivity in larger temperature range; 3) flexibility for both flat and sharp distributions in shape and magnitude; 4) better reconstruction stability over a wide range of noise levels.

In this letter, optical arrangement geometry for the tomography reconstruction is investigated in a certain domain of interest (Fig. 1). For the 8×8 discretization configuration, there are 128 variables, including 64 unknown concentration values and 64 unknown temperature values. Two asymmetric views are arranged around the domain, containing eight laser rays parallel to the grid in view 1 and 15 rays passing through the grid at an angle of 45° in view 2. The collimated laser beam is launched through gas medium and the laser intensity attenuation can be calculated according to the Beer–Lambert law. The absorbance for the discretization expression can be written as

$$\begin{aligned} A_{v_i,j} &= \sum_{m=1}^{M}\sum_{n=1}^{N}\left[PS_{v_i}(T)X\right]_{(m,n)} L_{(m,n),j} \\ &= \sum_{m=1}^{M}\sum_{n=1}^{N} a_{(m,n),v_i} L_{(m,n),j}\ (j=1,2,\cdots,J), \end{aligned} \tag{1}$$

where j is the index of the rays from reconstruction geometry and J is the total number of 23 rays from the two views; m and n are the index of row and column in the discretization grids by the size of M×N. The absorption coefficient $a_{(m,n),v_i}$, contains the parameters of line strength $S_{v_i}(T)$, mole fraction X, and total pressure P. $L_{(m,n),j}$ is the path length of the grid (m, n) passed through by ray j, and $A_{v_i,j}$ represents the integrated absorbance across the transition at wavelength v_i along the ray j. In this letter, the adaptive algebraic reconstruction technique (AART) is utilized to solve linear Eq. (1) in iterative equations[13]. A necessary complementarity to the solution of inversion problem in ill-posed Eq. (1) is the priori constraint. Based on the fact that gas distributions are continuous in combustion exhaust due to strong diffusion and mixing, the smoothness regularization has played an important role in reducing discrepancy of absorbances in adjacent grids, especially for the reconstruction with incomplete projections[9]. Smoothness factor δ represents the relative weight of absorbances calculated from target grid and its nearest neighbors. Physically, the magnitude of δ reflects the uniformity of absorbances distribution. Considering the existence of both flat and sharp distributions in dynamic combustion, δ with fixed value cannot be applied directly to describe the features in complicated situations without precise estimate in advance. Smaller δ would try to flatten the reconstructions. Here, self-adaptive smoothness regularization is suggested to adjust the factor δ automatically during iterations. This novel smoothness regularization is shown as

$$a_{(m,n),v_i} = \delta \times a_{(m,n),v_i} + (1-\delta)\times\left[\sum_{y=n-1}^{n+1}\sum_{x=m-1}^{m+1} a_{(x,y),v_i} H(a_{(x,y),v_i})\right] / 8. \tag{2}$$

According to the principle that peak containing larger absorbance in the distribution should dominate in Eq. (2) with less effect from neighbors, the magnitude of δ is scaled by comparison of absorbances in the target grid and its neighbors adaptively during iterations defined as

$$\delta = k\frac{a_{(m,n),v_i}}{\sum_{y=n-1}^{n+1}\sum_{x=m-1}^{m+1} a_{(x,y),v_i}}, \tag{3}$$

where k is the scaling constant. $H(a_{(x,y),v_i})$ is the correction function to compensate for the loss of peak value caused by average from its nearest neighbors.

$$H(a_{(x,y),v_i}) = 1 - \frac{\left(H(a_{(x,y),v_i}) - H(a_{(m,n),v_i})\right)}{a_{v_i}^{\text{theory}}}, \tag{4}$$

where $a_{v_i}^{\text{theory}}$ is the maximum absorbance in combustion at wavelength v_i in theory. On the other hand, the definition of smoothness factor is in accordance with the fact that larger relative error usually appears in the grid with small absorbance during incomplete reconstruction with noisy projections, where smaller δ should be adapted for absorbance average from neighbors to depress the reconstruction error. The function of the self-adaptive smoothness regularization would be introduced further in the detailed analysis of the reconstruction later. Other priori constraints, such as nonnegative boundary, are common which absorbances have to be subject to, and are not described here.

The advantage of two-wavelength scheme[1,2] is the ability to infer the gas temperature without knowing other parameters, such as concentration, pressure, and path length. However, the line strengths ratio of two transitions decreases with increase in temperature, resulting in the significant restriction of two-wavelength

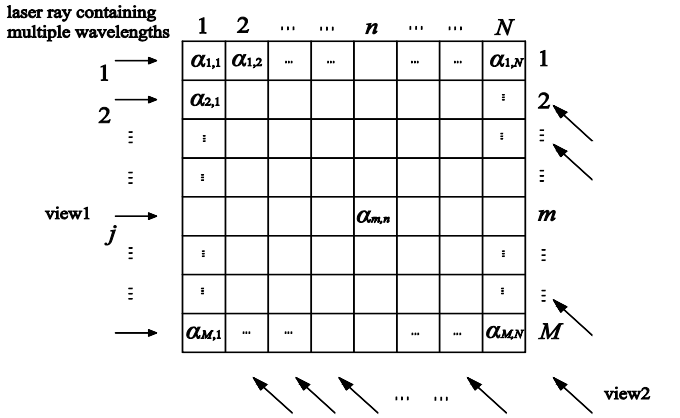

Fig. 1. Optical arrangement for SAATA and definition of discretization configuration.

scheme in a specific temperature range, which depends on the difference in the lower state energy of two transitions to ensure enough temperature sensitivity and signal-to-noise ratio in absorption detection. In this letter, a multiple wavelengths thermometry is proposed to infer the gas temperature covers a much larger temperature range. The novel regularization for adaptive ratio selection is defined here to adjust the proportion of ratios from line pairs to adapt for dynamic temperature automatically without more computation as

$$T_{(m,n)} = \sum_{i=1}^{I} \sum_{j=1}^{I} T_{(m,n),(v_i,v_j)} \times K_{(v_i,v_j)}, \tag{5}$$

where $T_{(m,n)}$ represents the calibrated temperature in the grid (m,n); $T_{(m,n),(v_i,v_j)}$ is the calculated temperature by two-wavelength scheme at wavelength v_i and v_j. $K_{(v_i,v_j)}$ is the normalization form of $k_{(v_i,v_j)}$, which is defined as ratio proportional control coefficient to provide the importance of the specific line pair in the determination of optimal temperature; I is the total number of wavelengths in calculation. Based on the trend of line strength ratio with increasing temperature, $k_{(v_i,v_j)}$ is expressed in logarithmic form as

$$k_{(v_i,v_j)} = \frac{1}{\left|\log R_{(v_i,v_j)} - A\right|^B}, \tag{6}$$

$$K_{(v_i,v_j)} = \frac{k_{(v_i,v_j)}}{\sum_{i=1}^{I} \sum_{j=1}^{I} k_{(v_i,v_j)}}, \tag{7}$$

where $R_{(v_i,v_j)}$ is the line strengths ratio at wavelengths of v_i and v_j. A and B are the location and width factors of the acceptable ratio range. The proposal of $k_{(v_i,v_j)}$ is to divide the whole temperature range, 300–3000 K, into several zones according to the available ratios as shown in Fig. 2. Specific ratio located in this zone should be dominant in determining the current temperature by Eqs. (5) and (7) due to the most suitable sensitivity.

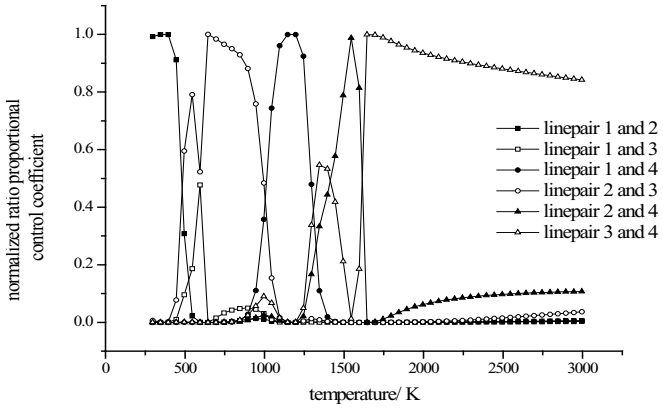

Fig. 2. Distribution of ratio proportional control coefficients in the temperature range from 300 to 3000 K.

The effect of factors A and B on ratio proportional control coefficients will be discussed in detail in following research.

For the multiple wavelengths measurement, the concentration can be easily calculated with reconstructed absorbance at each wavelength and optimal temperature described above. Considering the errors existed in the reconstruction at each wavelength, optimal determination regularization should be developed to improve the accuracy in concentration. Based on the fact that larger relative error usually appears in the grid with small absorbance, line strength is treated as the criterion to estimate precise concentration. Similar to the optimal temperature determination, regularization for adaptive line strength selection is proposed to adjust the proportion of the calculated concentration at each wavelength as

$$X_{(m,n)} = \sum_{i=1}^{I} X'_{(m,n),v_i} \times H_{v_i}, \tag{8}$$

$$H_{v_i} = \frac{S_{v_i}}{\sum_{i=1}^{I} S_{v_i}}, \tag{9}$$

where $X_{(m,n)}$ represents the calibrated concentration in the grid (m,n); $X'_{(m,n),v_i}$ is the calculated concentration at wavelength v_i. The key parameter, H_{v_i}, is the corresponding line strength proportional control coefficient, which is utilized to estimate the importance of line strength at specific temperature among the wavelengths. The contributions to concentration from all wavelengths would be helpful to depress the noise. Moreover, the calculated concentration from the strongest line strength would play the most important role in determination of optimal concentration. WDM method is utilized in this letter to extend the absorption information in each projection by line-of-sight measurement. Considering reliable laser performance and reasonable price for further application, four candidate wavelengths are chosen from the range of 1.3–1.5 μm. The spectroscopic parameters of candidates are listed in Table 1.

Process of SAATA is summarized and illustrated as follows. SAATA first deals with the noisy projections

Table 1. Spectroscopic Data for Tomography Reconstruction

	Wavelength (nm)	S_0 (cm^{-1}/atm)	E'' (cm^{-1})
1	1353.156	8.53×10^{-2}	446.5
2	1391.674	1.97×10^{-2}	1045.1
3	1343.297	5.4×10^{-4}	1774.8
	1343.299	5.76×10^{-4}	1806.7
4	1468.897	1.02×10^{-6}	3319.4

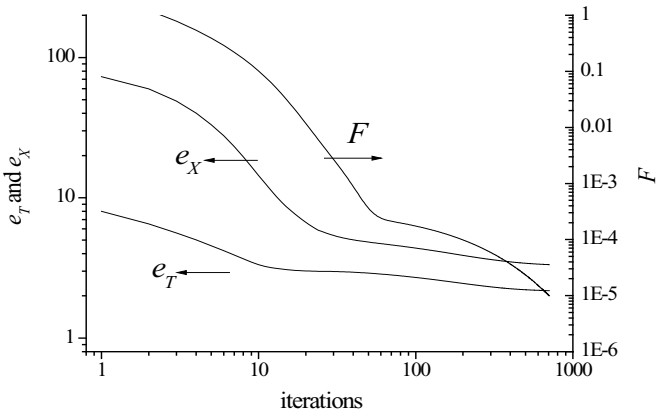

Fig. 3. Evolution of the value of F, average deviation e_X, and e_T during iterations by SAATA.

at multiple wavelengths and obtains the elementary reconstruction of absorbance distribution, where traditional two-wavelength scheme stops to offer the final results. The introduction of self-adaptive smoothness regularization would help to depress the reconstruction noise and refine the solutions further. In the next step, temperature distribution is reconstructed according to the multiple wavelengths thermometry in Eq. (5). This improved temperature distribution is utilized to calculate the line strength at each wavelength over each grid, leading to an improvement on concentration distribution by Eq. (8). Then a retrieval of absorbance is obtained by Beer–Lambert law to renew the elementary values and iteration continues until both concentration and temperature distribution results become steady.

The parameter F is defined as the criterion to observe the convergence of reconstruction process by the SAATA method. The agreement between reconstructions and phantoms is quantified by maximum and average deviations with normalized mean absolute distance, e_T and e_X, which is introduced in detail elsewhere[13].

$$F = \sum_{i=1}^{I} \frac{\sum_{n=1}^{N}\sum_{m=1}^{M}\left(\frac{\left|\alpha^{k-1}_{(m,n),v_i} - \alpha^{k}_{(m,n),v_i}\right|}{\alpha^{k}_{(m,n),v_i}}\right)}{M \times N}. \quad (10)$$

Minimization process of F and average deviations is shown in Fig. 3. The SAATA method starts the reconstructions with the initial absorbance distribution from back projection at each wavelength, and reduces e_T and e_X in each iteration gradually. Generally, e_T and e_X decreases in the same trend with decrease in F. However, the changes for both e_T and e_X are not linearly dependent on the iteration numbers, leading to an obvious inflection in the curve around 20 iterations. Before the inflection, the SAATA method shows extremely high efficiency in convergence, corresponding to the reduction from 8.2% to 3.6% in e_T and from 73.2% to 6.4% in e_X. The maximum deviations in temperature and concentration distributions are 147.8 K and 6.4%, respectively. After the inflection, the computation is increased sharply due to the slow convergence to final solution with desired accuracy. The algorithm terminates when the change in F is less than 1×10^{-5}, and the corresponding change in temperature and concentration is less than 6.0×10^{-3} K and 1.4×10^{-4}%. e_T of 2.2% is obtained finally from the reconstructed absorbance distribution. The algorithm completes the reconstruction when e_X of 3.4% is inferred in this example at last. Due to the nonlinear dependence of temperature on absorbance in Eq. (1), both variation amplitude and final value in e_T are smaller than e_X.

More than five phantoms of temperature and concentration distributions are used to verify the tomography reconstruction by the abovementioned SAATA method. These distribution phantoms are created by superimposing one or two Gaussian peaks on a paraboloid to simulate the asymmetric distribution of combustion exhaust encountered in practical engine or burner. One of the main advantages of the SAATA method is the adaptability to reconstruct combustion profiles in a much larger temperature range, which is vitally important for the running of combustion device under different conditions. Studies are performed to verify the ability of the SAATA method by simulations which consist of single inhomogeneity with Gaussian distribution describing temperature phantom by soft edges. The peak of the phantom, with the highest temperature

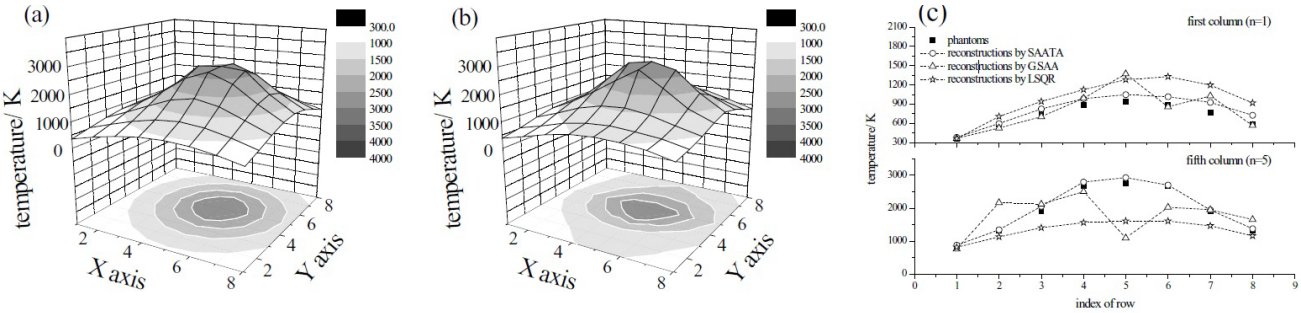

Fig. 4. (a) Temperature phantom in the range from 300 to 3000 K, (b) reconstructed temperature distribution with 0.5% noise in projections, and (c) comparison between phantoms and reconstructions by SAATA, GSAA, and LSQR methods along the first and fifth columns of the grids with 0.5% noise in projections.

of nearly 3000 K, locates in the center of the domain representing the core in combustion. Margins in the phantom influenced by the effect of boundary condition are defined below 1000 K, including the corners with lowest temperature of about 300 K. With 0.5% random white noise contained in projections, the reconstructed temperature distribution profiles are shown in Fig. 4. A significant agreement is achieved between the reconstructions and the phantoms, including the location and shape of peaks in temperature and concentration distributions.

A hybrid algorithm based on GSAA[18] is introduced to obtain the global optimization for comparison. Another method, least-square orthogonal-triangular decomposition (LSQR) which is very suitable for the solution of the ill-posed matrix equation, is also accepted here to reconstruct the phantom simultaneously. With the same optical arrangements, two-wavelength scheme (marked 2 and 3 in Table 1) is utilized for comparison algorithm here to infer gas temperature in 1000–2000 K due to its enough sensitivity in previous research. As can be seen in Fig. 4, in the temperature range of 300–1200 K, the deviations in the temperature reconstruction are within 127 K by the SAATA method, much less than 263 K by the GSAA method and 463 K by the LSQR method. Similar results are observed in the temperature range up to 3000 K. Corresponding average deviations e_T is 7.8% with regard to 20.4% and 22.7% by comparison methods, respectively. The SAATA method can reconstruct the accurate phantoms details at both less than 1000 K and more than 2000 K due to the satisfactory sensitivity in a much larger temperature range through the regularization of adaptive ratio selection in Eq. (6). Here, location factor A plays an important role in determination of specific ratio which should be considered to infer the temperature dominantly. The function of adaptive ratio selection is to maintain the temperature measurement with the suitable ratio over the whole temperature range from 300 to 3000 K. The contribution of line strength ratio to corresponding ratio proportional control coefficient $K_{(v_i,v_j)}$, for single specific line pair with different location factor A, is shown in Fig. 5.

With reasonable decrease in parameter A, the peak of $K_{(v_i,v_j)}$ moves forward to the high-temperature zone, where this specific ratio dominates and is utilized to infer the temperature. Obviously, the appropriate value of A should perform a uniform distribution of ratio proportional control coefficients from all transitions to cover the whole temperature range (300–3000K) with high sensitivity, and 0.4 is suggested to be a suitable value in this letter according to the comparison of reconstruction simulation. Parameter B represents the width of temperature determination zone by the specific ratio. Increase in B would broaden the zone and reduce the influence of ratios from other absorption line pairs. For example, $K_{(v_i,v_j)}$ exceeds 0.8 at the temperature zone from 815 to 1209 K with value of 4 for parameter B. However, this zone would be narrowed from 891 to 971 K when B is set for 1. A combination of $K_{(v_i,v_j)}$ from other ratios would occupy the remaining zones and determine the temperature together. In this letter, 1 is suggested to be adopted for B.

A double peaks phantom is created to demonstrate the ability to capture the peaks by the SAATA method (Fig. 6). An appropriate temperature range from 1000 to 2000 K would guarantee satisfactory temperature sensitivity for all the tomography reconstruction methods. The comparison shows that SAATA method can perform better reconstructions and capture the shape and magnitude of the phantoms quite accurately, which owes much to its self-adaptive smoothness regularization. The maximum deviation in this column is up to 394 K by the GSAA method and 262 K by the LSQR method, and corresponding average deviation of e_T closes up to 12.7% and 13.4%.

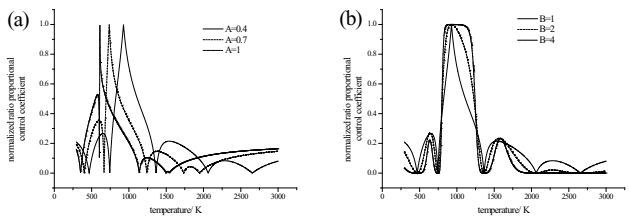

Fig. 5. Effect of (a) location factor A and (b) width factor B on ratio proportional control coefficients for line pair at wavelengths 1391.7 and 1343.3 nm.

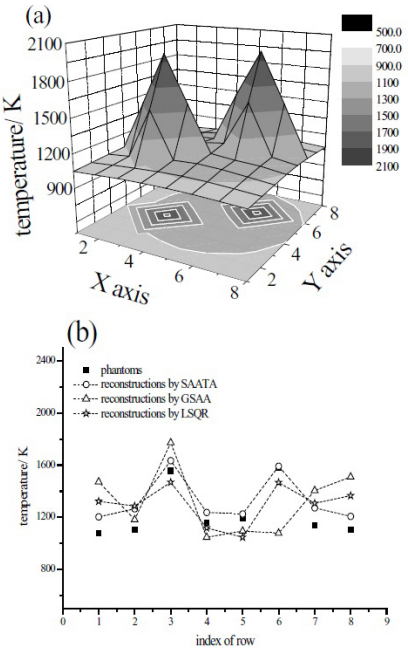

Fig. 6. (a) Double peaks phantom and (b) comparison between double-peak phantoms and reconstructions by SAATA, GSAA, and LSQR methods along the fourth column of the grids with 0.5% noise in projections.

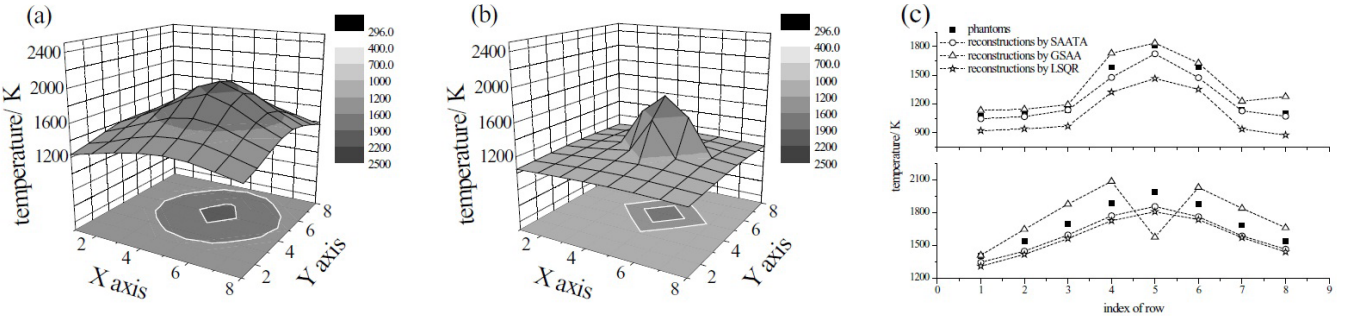

Fig. 7. (a) Flat temperature distribution phantom, (b) sharp temperature distribution phantom, and (c) comparisons between phantoms and reconstructions by SAATA, GSAA, and LSQR methods along the fourth column of the grid with 0.5% noise in projections.

However, the deviations are within 161 K by the SAATA method, and average deviation of e_X decreases to 7.8%.

For better explanation about the function of the regularization, another reconstruction is carried out to verify the adaptability of the SAATA method to both flat and sharp distributions, which is another advantage of the SAATA method essential for combustion diagnosis in startup and running process. Figure 7 provides a comparison of phantoms and the reconstructions.

Again, the temperature range of phantoms is still assumed from 1000 to 2000 K to guarantee enough temperature sensitivity for all the tomography reconstruction methods. The self-adaptive smoothness regularization offers sufficient elasticity to accommodate both kinds of distributions for the SAATA method. In the case of sharp distribution, the smoothness regularization factor of δ increases to 0.99 near the sharp peak and reduces to 0.95 at the flat margin. As a result of this self-adaptive adjustment in δ, the SAATA method significantly reduces average deviation of e_T to 4.5%, much less than 6.3% by the GSAA method and 10.5% by the LSQR method. Similar self-adaptive adjustment in δ, ranged from 0.93 to 0.96, is observed in the reconstruction process of flat distribution phantom. The maximum deviation at the peak reduces to 132 K, a great improvement in description of peak value with deviation of 412 K by the GSAA method and 181 K by the LSQR method.

Another demonstration is the reconstruction of the phantom with extensive null-space. The 40×40 discretization configuration, totally 1600 grids, is adopted with the same optical arrangement of 23 rays. The phantoms and reconstructions are shown in Fig. 8. About 8% of the domain is covered by the target gas. Obviously, most grids are not passed through by the limited laser rays and would be inferred by the smooth regularization only. SAATA can obtain better results in the determination of both concentration and temperature distribution locations, but the shape and value are distorted slightly by the smooth function, resulting in e_X of 37.2% and e_T of 7.7%. More importantly, temperature can be inferred from this much noisy absorption distribution with extensive null-space due to the optimal temperature determination over a larger temperature range.

The stability of the SAATA method is studied by reconstruction of temperature and concentration distributions when projection measurements contain random white noise. The typical values for a minimum detectable absorbance in direct measurement are 1×10^{-4}, representing the precise measurement subjected to fundamental noise, and 1×10^{-3}, representing the measurements influenced by larger noise source. For a combustion device with size of 8×8 (cm) in cross-section, corresponding noise level ranged from 1% to 10% in projections are utilized to simulate the measurement in the practical environment. Ten reconstructions are performed at the same noise level to yield the average deviation of e_T and e_X (Fig. 9). The SAATA method outperforms the GSAA method in both temperature and concentration reconstructions. At noise levels below 1%, the e_T and e_X by the SAATA method are 2.5% and 4.0%, much less than the corresponding values of 4.7% and 8.5% by the GSAA method. In contrast to the faster trend of e_T and e_X by the GSAA method,

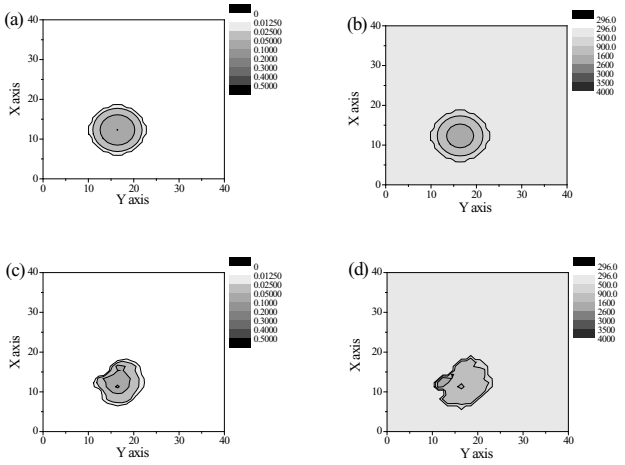

Fig. 8. (a) Concentration phantom, (b) temperature phantom with extensive null-space, (c) reconstructed concentration distribution, and (d) reconstructed temperature distribution.

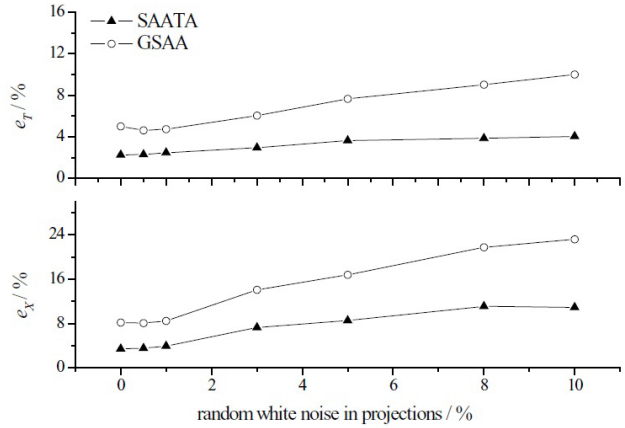

Fig. 9. Comparison of average deviations e_X and e_T in reconstructions by SAATA and GSAA methods at noise levels from 1% to 10% in projections.

e_T and e_X increase with the noise level much slowly by the SAATA method. The SAATA method yields reconstructions less sensitive to the projection noise. These results demonstrate that SAATA method can perform much better reconstruction with noisy projections than other two-wavelength methods, especially for the temperature reconstructions due to its nonlinear dependence on absorbance and high sensitivity in larger temperature range. Of course, the reconstruction quality would be expected to be improved further with more wavelengths multiplexed or projections introduced into the optical arrangement when the limitations on practical applications are overcome.

In conclusion, a novel self-adaptive algebraic tomography algorithm is developed to investigate the simultaneous tomography reconstruction of concentration and temperature distribution based on multiple wavelengths absorption spectroscopy. The extension of spectral information at multiple wavelengths enables a simplified optical arrangement with fewer projections from two views. The significant virtues of the method include flexibility to simultaneously reconstruct concentration and temperature distribution in the range from 300 to 3000 K, and maintain high temperature sensitivity by self-adaptive adjustment behavior. A variety of phantoms are investigated to demonstrate the ability of SAATA method to capture the shape and magnitude for both flat and sharp distribution. In consideration of advantages including the hardware cost, system complexity, adequate temporal resolution, and reasonable computation, the introduced optical arrangement and the method here result in great potential in applications of practical combustion diagnosis.

This work was supported by the National Natural Science Foundation of China (No. 11372141), the Specialized Research Fund for the Doctoral Program of Higher Education of China (No. 20113219120045), and the Fundamental Research Funds for the Central Universities (No. 30920130112007).

References

1. X. Zhou, X. Liu, J. B. Jeffries, and R. K. Hanson, Meas. Sci. Technol. **14,** 1459 (2003).
2. J. T. C. Liu, J. B. Jeffries, and R. K. Hanson, Appl. Phys. B **78,** 503 (2004).
3. R. Qi, Z. Du, D. Gao, J. Li, and K. Xu, Chin. Opt. Lett. **10,** 033001 (2012).
4. G. Tu, Y. Wang, F. Dong, H. Xia, T. Pang, Z. Zhang, and B. Wu, Chin. Opt. Lett. **10,** 042801 (2012).
5. E. J. Beiting, Opt. Lett. **16,** 1280 (1996).
6. S. J. Carey, H. McCann, F. P. Hindle, K. B. Ozanyan, D. E. Winterbone, and E. Clough, Chem. Eng. J. **77,** 111 (2000).
7. B. Gillet, Y. Hardalupas, C. Kavounides, and A. M. K. P. Taylor, Appl. Therm. Eng. **24,** 1633 (2004).
8. N. Terzija, J. L. Davidson, C. A. G. Stewart, P. Wright, K. B. Ozanyan, S. Pegrum, T. J. Litt, and H. McCann, Meas. Sci. Technol. **19,** 094007 (2008).
9. M. G. Twynstra and K. J. Daun, Appl. Opt. **51,** 7059 (2012).
10. J. L. Song, Y. J. Hong, H. Pan, and G. Y. Wang, Proc. SPIE **8907,** (2013).
11. P. Wright, N. Terzija, J. L. Davidson, S. G. Castillo, C. G. Stewart, S. Pegrum, S. Colbourne, P. Turner, S. D. Crossley, T. Litt, S. Murray, K. B. Ozanyan, and H. McCann, Chem. Eng. J. **158,** 2 (2010).
12. K. J. Daun, J. Quant. Spectrosc. Radiat. Transfer **111,** 105 (2010).
13. N. Li and C. Weng, Chin. Opt. Lett. **9,** 061201 (2011).
14. M. G. Twynstra, K. J. Daun, and S. L. Waslander, J. Quant. Spectrosc. Radiat. Transfer **143,** 25 (2014).
15. S. T. Sanders, J. Wang, J. B. Jeffries, and R. K. Hanson, Appl. Opt. **40,** 4404 (2001).
16. N. Li, J. H. Yan, F. Wang, Y. Chi, and K. F. Cen, Spectrosc. Spect. Anal. **28,** 1708 (2008).
17. L. Ma and W. W. Cai, Appl. Opt. **47,** 3751 (2008).
18. N. Li and C. S. Weng, Acta Phys. Sin. **59,** 6914 (2010).